AU8808962

ANSTO/E672

ANSTO/E672

AUSTRALIAN NUCLEAR SCIENCE AND TECHNOLOGY ORGANISATION

LUCAS HEIGHTS RESEARCH LABORATORIES

ROTAMAK EQUILIBRIUM CALCULATIONS USING THE PEST CODE

by

P.A. WATTERSON

DECEMBER 1987

ISBN 0 642 59875 2

AUSTRALIAN NUCLEAR SCIENCE
AND TECHNOLOGY ORGANISATION

LUCAS HEIGHTS RESEARCH LABORATORIES

ROTAMAK EQUILIBRIUM CALCULATIONS USING THE PEST CODE

by

P.A. WATTERSON

ABSTRACT

This report describes the use of the equilibrium part of the Princeton equilibrium and stability code PEST to model rotamak equilibria with an applied toroidal magnetic field. An overview of the code is provided, together with a list of the required input data. The simulation of a range of equilibria measured in the ANSTO rotamak shows that the rotamak approximately satisfies magnetohydrodynamic equilibrium. Of particular interest is the presence of large diamagnetic poloidal current about the magnetic axis which produces a peak in the plasma pressure on the magnetic axis. For a low toroidal field, however, poloidal current of opposite direction is simultaneously driven on flux surfaces distant from the magnetic axis, producing paramagnetism.

National Library of Australia card number and ISBN 0 642 59876 2

The following descriptors have been selected from the INIS Thesaurus to describe the subject content of this report for information retrieval purposes. For further details please refer to IAEA-INIS-12 (INIS: Manual for Indexing) and IAEA-INIS-13 (INIS: Thesaurus) published in Vienna by the International Atomic Energy Agency.

COMPUTER CALCULATIONS; ELECTRIC CURRENTS; MAGNETIC FIELDS; MAGNETIC FLUX; MHD EQUILIBRIUM; P CODES; PLASMA; PLASMA PRESSURE; ROTAMAK DEVICES; STABILITY; TOROIDAL CONFIGURATION

The Australian Nuclear Science and Technology Organisation replaced the Australian Atomic Energy Commission on 27 April 1987. Reports issued after April 1987 have the prefix ANSTO with no change of the symbol (E, M, S or C) or numbering sequence.

CONTENTS

1. INTRODUCTION

In standard rotamak experiments, a steady toroidal current is driven in a spherical plasma by the application of a rotating magnetic field [Hugrass *et al.* 1980, Durance *et al.* 1982]. Previously, the steady poloidal magnetic field associated with this current has been approximately modelled by solutions of the pressure balance equation

$$\mathbf{J} \times \mathbf{B} = \nabla p \tag{1}$$

with the plasma pressure p proportional to a power of the poloidal magnetic flux function [Storer 1982, 1983]. By allowing a more general form for p, a better fit was obtained for the ANSTO rotamak, in which pressure was also experimentally determined [Durance *et al.* 1987].

In a recent experiment on the ANSTO rotamak [Collins *et al.* 1987], a steady toroidal field was added by passing a current through a conductor along the central axis. If this toroidal field maintained its vacuum profile, it would have no effect on pressure balance. Instead, however, steady poloidal currents were driven which combined with the toroidal field to contribute another term to the Lorenz force. A detailed report on the modelling of the equilibria obtained for a range of toroidal field values is now provided.

The calculations were made using a modified version of the equilibrium part of the Princeton equilibrium and stability code PEST [Johnson *et al.* 1979]. The problem solved is described in **section 2** below, and an outline of the code is given in **section 3**. This is followed by a list of the input data, and a guide to the code output. The results of modelling the ANSTO rotamak are shown in **section 6**. Finally, some auxiliary computer programs for analysing the experimental data are described in **appendix A**.

2. THE EQUILIBRIUM PROBLEM

The axisymmetric solutions of the **pressure balance equation 1** are the solutions of the Grad-Shafranov equation (in cylindrical co-ordinates (X,ϕ,Z)),

$$X \frac{\partial}{\partial X}\left[\frac{1}{X}\frac{\partial \Psi}{\partial X}\right] + \frac{\partial^2 \Psi}{\partial Z^2} = 2\pi X \mu_0 J_\phi \quad , \tag{2}$$

$$\mu_0 J_\phi = -2\pi\left[X\mu_0 \frac{dp}{d\Psi} + \frac{R^2 B_0^2}{X} g \frac{dg}{d\Psi}\right] \quad , \tag{3}$$

where Ψ is the poloidal flux function, satisfying

$$B_x = \frac{1}{2\pi X}\frac{\partial \Psi}{\partial Z} \quad , \quad B_z = -\frac{1}{2\pi X}\frac{\partial \Psi}{\partial X} \quad , \tag{4}$$

p and g are functions of Ψ, and

$$B_\phi = \frac{R B_0 g}{X} \quad , \tag{5}$$

where B_0 is the magnitude at X = R of the applied (or 'vacuum') toroidal field, B_ϕ^{vac}. The departure of g from 1 is related to the poloidal plasma current I_{pol} (defined for each (X,Z) by the current passing through the disc bounded by the circle X,Z, $0 \le \phi \le 2\pi$) by

$$I_{pol} = \frac{2\pi}{\mu_0} X\left[B_\phi - B_\phi^{vac}\right] = \frac{2\pi}{\mu_0} R B_0 (g-1) \quad . \tag{6}$$

In the ANSTO rotamak, the plasma occupies a spherical glass vessel except for a narrow glass tube along the symmetry axis (containing the conductors by which B_ϕ^{vac} is applied). As illustrated in **figure 1**, the equilibrium configuration typically has a region of closed poloidal field lines surrounded by a sheath of open field lines which pass through the vessel wall. Significant plasma pressure and J_ϕ is observed on these open field lines.

The functional forms adopted for dp/dΨ and g, incorporating non-zero p outside the separatrix, are

$$\Psi < 0\,, \qquad \frac{dp}{d\Psi} = c\left[1 + \delta(\Psi/\Psi_a)^{\alpha-1}\right]\,, \tag{7}$$

(Inside the separatrix)
$$g = 1 + \gamma_1(\Psi/\Psi_a)^{\beta_1} - \gamma_2(\Psi/\Psi_a)^{\beta_2}\,, \tag{8}$$

$$\Psi > 0\,, \qquad \frac{dp}{d\Psi} = c\left[1 - \Psi/\Psi_l\right]\,, \tag{9}$$

(outside the separatrix)
$$g = 1\,, \tag{10}$$

where Ψ_a is Ψ at the magnetic axis, Ψ_l is Ψ at the vessel wall at $Z = 0$, and c is scaled so that I_ϕ equals its experimental value. The forms chosen for $\Psi > 0$ are such that J_ϕ drops almost linearly outside the separatrix to zero at the vessel at $Z = 0$. For all points outside the vessel $J_\phi = 0$ is assigned. Use of $g = 1$ on $\Psi > 0$ implies $J_{pol} = 0$ outside the separatrix, avoiding charge build-up where the open field lines intersect the vessel. To obtain $p(\Psi)$, $dp/d\Psi$ is integrated assuming $p = 0$ at the vessel at $Z = 0$. For $Z \neq 0$, the vessel supports the non-zero pressure on the open field lines.

The equilibrium problem is completed with the specification of the external field coils generating the 'vertical' field required for equilibrium. In this work the experimental coil location and field magnitude are used, in contrast to the modelling by Storer [1982, 1983] who varied the field magnitude in the calculated equilibria to improve the overall fit with experiment.

3. DETAILS OF THE PEST CODE

For those wishing to make even minor modifications to the PEST code, an overall knowledge of its operation is required. Although lists of input parameters are available [Manickam and McCann 1977, Dalhed 1978], there are no detailed guides to the code. The code contains few comments and the use of global common blocks makes most variables universal and hard to track down. **Sections 3.1** to **3.3** below record the basic features of the code, showing how we have modified it for application to the rotamak. Those who only wish to run the code should consult **section 3.4**.

3.1 Scaling

All variables used in the code are made dimensionless (denoted by prime below) *via* the scaling constants

$$XSC = R \qquad \text{for length,} \tag{11a}$$

$$CSC = 2\pi\mu_0/B_0 XSC \qquad \text{for (current)}^{-1}, \tag{11b}$$

$$PSC = B_0^2/\mu_0 \qquad \text{for pressure.} \tag{11c}$$

Thus, after the initial subroutine UNITS, the code employs variables $X' = X/XSC$, $Z' = Z/XSC$, $R' = R/XSC$ (= 1), $I_\phi' = CSC\ I_\phi$, $J_\phi' = XSC^2\ CSC\ J_\phi$, $\Psi' = \Psi/XSC^2\ B_0$, $p' = p/PSC$, *etc.* in terms of which the Grad-Shafranov **equation (2)-(3)** reads

$$X' \frac{\partial}{\partial X'}\left[\frac{1}{X'}\frac{\partial \Psi'}{\partial X'}\right] + \frac{\partial^2 \Psi'}{\partial Z'^2} = X' J_\phi'\,, \tag{12}$$

$$X' J_\phi' = -(2\pi)^2\left[X'^2 \frac{dp'}{d\Psi'} + g\frac{dg}{d\Psi'} R'^2\right]\,. \tag{13}$$

Rescaling (to SI units) is performed in the code only at places where variables are output.

3.2 Subroutines

Figure 2 is a flow chart which summarises the action of the PEST code, indicating the principal subroutines called by the main program. A more mathematical description of the code algorithm may be found in Johnson *et al.* [1979], along with definitions of the alternative flux surface label $\psi(\Psi)$ and the surface quantities $D_I(\Psi)$ and $D_R(\Psi)$, which indicate localised instability where positive. Other variables referred to are the safety factor $q(\Psi)$ and the total plasma energy $W_p = (3/2)\int p dV$. Subscript 'a' is used henceforth to

denote evaluation at the magnetic axis.

3.3 Modifications to the Code

Many modifications have been made to the original PEST code to apply it to rotamak equilibria. The foremost (and simplest) changes concern the functions p and g and their derivatives with respect to Ψ (denoted PP and DG in the code). The original practice of varying a parameter of g to give the desired I_ϕ has been changed — here $dp/d\Psi$ (and p) is scaled by c in **equations 7** and **9**. Thus, the maximum pressure is not known beforehand; instead control is exerted on the deviation of B_ϕ from B_ϕ^{vac}, which is more directly measured.

The presence of plasma outside the separatrix requires several new features in the code. The glass vessel radius is stored in PLIMRA(10) and, wherever J_ϕ is evaluated (particularly in STARTJ), it is set to zero outside the vessel. Flux surface quantities such as q are only applicable within closed flux regions, hence (in subroutines MAPPER and SUROUT) their domain is restricted to $\Psi \le 0$ (actually $\Psi \le$ PSIMAX $\equiv \Psi_a/20$ was used). Also formula (25) of Johnson *et al.* [1979], in which J_ϕ is evaluated in terms of surface quantities, is not applicable outside the separatrix (so in several places subroutine STARTJ is called instead of NEWJ).

An optional relaxation step in the iteration has been introduced for use when a calculation fails to converge but oscillates about an apparent equilibrium. In subroutine PSICHK, instead of adopting the new Ψ (returned by POISON) a weighted average of the new and old Ψ can be used. The weighting is governed by the relaxation parameter SMFAC (input in BL04, see **section 4**), with value 1 corresponding to no relaxation (used in all solutions reported in **section 6**), and value 0.5 recommended if an oscillation occurs.

3.4 Executing the Code

The source codes are stored on the Lucas Heights IBM mainframe computer in the partitioned data set PAW.EQUIL. The original (single precision) code lies in PEST1SPS whereas RUNCTG contains the subroutines which have been altered and the JCL to recompile any further changes. Compiled object codes are stored in PAW.PESTEQS, including the complete run module PROGPGM, which can be executed by the job PAW.EQUIL(RUNG).

4. INPUT DATA

The input data are read from unit 15 in 9 blocks using the NAMELIST facility. The most frequently changed parameters, associated with the p and g functions, are found in block 4. The functions as coded are

$$\Psi<0\,,\quad \frac{dp}{d\Psi} = c\left[1 - \text{DELP1}\,\Psi_n^{\text{EXPP1}-1} - \text{DELP2}\,\Psi_n^{\text{EXPP2}-1}\right]\,, \tag{14a}$$

$$g = 1 - \text{DELG}\,\Psi_n^{\text{EXPG}} - \text{DELG1}\,\Psi_n^{\text{EXPG1}}\,, \tag{14b}$$

$$\Psi>0\,,\quad \frac{dp}{d\Psi} = c\left[1 - (\Psi/\Psi_l)^{\text{EXPP}-1}\right]\,, \tag{14c}$$

$$g = 1\,, \tag{14d}$$

where $\Psi_n = \Psi/\Psi_a$. To reproduce **equations 7-10** set DELP1 $= -\delta$, EXPP1 $= \alpha$, DELP2 $= 0$ (making EXPP2 redundant), DELG $= -\gamma_1$, EXPG $= \beta_1$, DELG1 $= \gamma_2$, EXPG1 $= \beta_2$ and EXPP $= 2$. Other key parameters are listed below, with values recommended for the ANSTO rotamak given in square brackets. Modifications to the code have made certain parameters inapplicable, as indicated.

BL01 :

NDIM [65]	— grid dimension in both X and Z directions
NPA,NBA [25]	— maximum number of inner and outer loop iterations
NEC [1]	— number of external field coil pairs
NLCDS [1]	— number of limiters
NOSURF [25]	— number of closed flux surfaces used in mapping and q evaluation, *etc.*
KVF [0]	— for free boundary equilibrium
IQUIB [1]	— to allow option of a sequence of equilibria

	IVARY [1-4]	— number of equilibria required
	IQFUNC	— made inapplicable
BL02 :	RZERO [0.005]	— radius of inside edge of grid, corresponding (approximately) to inner glass tube radius
	ALR, ALZ [0.16,0.32]	— grid lengths in X and Z directions
	TCUR0	— I_ϕ
	B0, R	— B_ϕ^{vac} at X=R (recommend R = 0.10 m so that dimensionless lengths are easily interpreted)
BL03 :	P0 [1.0, or anything non-zero]	— initial guess for p scaling
BL04 :	EGUESS [3.0]	— exponent used in initial Ψ guess
	EPSPA, EPSBA [5×10^{-4}]	— convergence criteria
	IPOUT [1]	= 1 if $p \neq 0$ required outside separatrix (alternatives may be coded into p,g, *etc.*)
	SMFAC[1]	— relaxation parameter in iteration
	DDELP1	— increment to DELP1 imposed by VARY
	DDELG	— increment to DELG imposed by VARY
BL05 :	PEC(1:3,1) [Z_c, X_c, I_c]	— location and magnitude of pair of external current coils (second coil assumed at $Z = -Z_c$)
BL06 :	PLIMZA(1), PLIMZB(1) [0,0]	— left and right Z co-ordinates of limiter
	PLIMRA(1), PLIMRB(1) [0.14,0.145]	— left and right X co-ordinates of limiter
	PLIMRA(10) [0.14]	— glass vessel radius
BL07 :	NOLIM	— made inapplicable
	IPRNT [0]	— controls amount of printout
	IFUNC [7]	— controls choice of p and g functions; value 7 selects **equation 14**
BL09 :	ICEN [2]	— centre of initial Ψ guess is displaced by this number of grid points from centre of grid. Convergence can be very sensitive to its value.

For the calculation of equilibria with $B_\phi = 0$, an arbitrary fictitious B_ϕ^{vac} must be specified as it is used in scaling (see **equation 11**). If g is set at 1 (by DELG = DELG1 = 0) this B_ϕ^{vac} has no effect on pressure balance since $\mathbf{J}_{pol} = 0$, and the true $\mathbf{B}_{pol}$ and J_ϕ are obtained.

5. OUTPUT

5.1 Printed Output

As well as listing the input parameters and details of the equilibrium (if found), the output states the values of key variables (all dimensionless) at each step of the iteration. P0 gives the maximum p, RSEP and ZSEP give the locations of the separatrix on Z = 0 and X = 0, and JP and JG are the two terms of J_ϕ in **equation 13** at the magnetic axis. Also the values of Ψ and XJ_ϕ on Z = 0 at every fifth grid point are listed.

Included in the output describing the equilibrium are various β values. Because $B_\phi \sim 1/X$ as $X \to 0$, any β measure integrating B_ϕ^2 yields a very low value which depends principally on how close the integration is taken to X = 0. The most useful β seems to be

$$\beta_{pol} = 2\mu_0 \int p dV \Big/ \int B_{pol}^2 \, dV \qquad (15)$$

(evaluated in subroutine ENERGY). Two values are given — for the integrals taken over the whole vessel and over just the region within the separatrix. The latter (a higher value) can be checked against the value determined in SUROUT by integrating over ψ. Since the field outside the separatrix helps to confine the

plasma, it is recommended that the value for the integrals over the whole vessel be used.

5.2 Graphical Output

The graphical output consists of the following plots:

Ψ and J_ϕ contour plots;

p, q, J_ϕ and $X(B_\phi - B_\phi^{vac})$ on $Z = 0$ *v.* X; and

D_I and D_R (mentioned in **section 3.2**), p, g and q *v.* ψ (which goes from 0 on the magnetic axis to 1 at $\Psi = \Psi_a/20$, near the separatrix).

5.3 Other Output

The code generates an output file (unit 10) containing values of J_ϕ, g, p, q and B_z at the grid points on $Z = 0$. This file is intended to be used as input for comparative plotting with experimental data.

Various details about the equilibrium (including Ψ) are also written to unit 17 (for use by a stability code) but at the present time this file is not saved. Nor is file 22, which stores a vector of values $q(\Psi)$.

6. RESULTS OF MODELLING THE ANSTO ROTAMAK

As reported by Collins *et al.* [1987], equilibria in the ANSTO rotamak have been obtained for a range of applied B_ϕ^{vac}, namely B_ϕ^{vac} = 0, 22, 79, 114 and 148 G at R = 10 cm, labelled *Cases 1* to *5*. Further information is now provided about the solutions developed to model these equilibria.

Initially it was hoped that the selection of $dp/d\Psi$ and g for each equilibrium could be fully automated by employing the program PGPROG described in **appendix A**. This program determined $dp/d\Psi$ and g of **form 14** to reproduce the experimental J_ϕ. When the PEST code failed to converge for these functions, the form for $dp/d\Psi$ was simplified by neglecting the DELP2 term in **equation 14a**, and the parameter values for g were modified so as to better fit the observed I_{pol} (g and I_{pol} being related by **equation 6**). Hereafter the parameters discussed are those in the more concise **expressions 7-10**.

In all cases with a toroidal field, a high poloidal current loop was observed in the neighbourhood of the (magnetic) axis, with sign to confine pressure on the axis. This was included in g *via* the 'diamagnetic' term $-\gamma_2(\Psi/\Psi_a)^{\beta_2}$ with $\gamma_2 > 0$ and β_2 large. The confining effect was accounted for in $dp/d\Psi$ *via* $\delta(\Psi/\Psi_a)^{\alpha-1}$ with $\delta > 0$. By setting $\alpha = \beta_2$ the contributions to J_ϕ of the $dp/d\Psi$ and $dg/d\Psi$ terms associated with this diamagnetic core could be made to roughly cancel for the correct δ. For δ too large, excess J_ϕ was concentrated on the axis, causing it to expand in the numerical iteration and force the plasma onto the vessel. For δ too small, a region of negative J_ϕ appeared and the algorithm failed to converge. Within the window of convergence in δ, the maximum p (at the axis) decreased with decreasing δ, and to give closest agreement with the measured p, the smallest possible δ was used.

The parameter values finally arrived at are listed in **table 1**, and **figure 3** displays the agreement achieved between the measured and calculated equilibria. **Table 2** compares the experimental and calculated X_a, separatrix location X_s, maximum pressure p_a, and q_a, and also gives β_{pol} and W_p for the calculated equilibria. Based on the experimental power input P_{in} for each case, the energy confinement time $\tau_E = W_p/P_{in}$ is deduced, typically of the order 5 μs. A failing common to all the models is that they have slightly large magnetic axis and separatrix locations (by 1-2 cm), possibly because of the neglect of the radial confinement by the ponderomotive forces. This could also explain why the measured pressure slightly exceeds the calculated pressure in all cases. Comments specific to each equilibrium are given below.

Case 1 - For this zero B_ϕ case, the observed dip in J_ϕ on the axis must be associated with a dip in $dp/d\Psi$ there. It is remarked that if the vertical field is increased by 20 per cent to simulate additional confinement by the ponderomotive pressure of the rotating magnetic field, then the separatrix shifts inwards to equal its experimental value and p_a rises to 20 Pa.

Case 2 - This equilibrium is paramagnetic everywhere ($B_\phi > B_\phi^{vac}$) but note that I_{pol} dips near the axis; equivalently J_{pol} reverses sign from the outer closed flux surfaces to the inner surfaces near the

axis. The magnitude of the poloidal currents were reduced by 30 per cent in the calculation as this improved the fit of the J_ϕ profile.

Case 3 - Once again, paramagnetism is observed in the outer flux surfaces, but near the axis large reversed $\mathbf{J}_{pol}$ brings B_ϕ to below B_ϕ^{vac}, causing diamagnetism. It was necessary to diminish the poloidal currents to produce reasonable modelling of J_ϕ and also to keep the calculated p below the experimental value. A more extensive parameter search (or more general functional forms for $dp/d\Psi$ and g) might improve the overall fit. However, for cases like *2* and *3* with poloidal currents in both directions, the numerical iteration is very sensitive to all parameters and initial conditions, and convergence is hard to find.

Cases 4 and 5 - Both these large B_ϕ equilibria feature strong diamagnetic poloidal currents about the magnetic axis, which have been accurately simulated. Both the experimental and calculated equilibria feature peaking of the pressure at the magnetic axis, due to this poloidal current.

For each calculated equilibrium with non-zero B_ϕ, the safety factor q increased from a minimum on the magnetic axis to infinity on the separatrix. The agreement with the experimental axis value was good (see **table 2**) except for *Case 2* in which poor fitting of J_ϕ near the axis resulted in a calculated q_a of 0.7, compared to the experimental q_a of 2.1. For *Cases 3* to *5*, q_a exceeded unity. With regard to the profiles of D_I and D_R for the calculated equilibria, the following general rule was observed: for $q_a < 1$, surfaces from the magnetic axis out to $q \approx 1$ were unstable ($D_I > 0$ and $D_R > 0$, with the region $D_R > 0$ slightly larger) beyond which they were stable; and for $q_a > 1$ all surfaces were stable. Thus the calculated *Case 2* equilibrium was the only unstable one from *Cases 2* to *5*, but the higher experimental q_a suggests that, in fact, *Case 2* was also stable. *Case 1* with $q \equiv 0$ was unstable (at least D_I and D_R approached positive infinity when the stability was calculated with a small B_ϕ approaching zero).

7. CONCLUSIONS

The general agreement obtained between the experimental and model equilibria is good, indicating that the plasma was close to satisfying pressure balance. To obtain this agreement it was necessary to include toroidal current, but not poloidal current, outside the separatrix. Within the separatrix, the poloidal currents were diamagnetic near the magnetic axis but paramagnetic further away from the axis for low toroidal field values. The safety factor q, deduced from the calculated equilibria with toroidal field, increased from a minimum value around 1-2 on the magnetic axis to large values near the separatrix, making the field configuration that of a compact tokamak.

Further theoretical studies should be undertaken on the global stability of the equilibria, and on how both paramagnetic and diamagnetic poloidal currents are driven by the rotating magnetic field.

8. ACKNOWLEDGEMENTS

The author would like to thank G. Durance for providing the experimental data, I.J. Donnelly for many valuable discussions and B.E. Clancy for computing assistance. The late R.C. Grimm established the PEST code at Lucas Heights and made some of the necessary modifications, with the assistance of E.K. Rose.

9. REFERENCES

Collins, G.A., Durance, G., Hogg, G.R., Tendys, J., Watterson, P.A. [1987] - Small aspect ratio tokamak configurations generated by rotating magnetic field current drive. *Nucl. Fusion* (in press).

Dalhed, S. [1978] - Users' Manual for the Princeton Code. Princeton University, Plasma Physics Laboratory.

Durance, G., Hogg, G.R., Tendys, J., Watterson, P.A. [1987] - *Plasma Phys. Control. Fusion*, 29:227.

Durance, G., Jessup, B.L., Jones, I.R., Tendys, J. [1982] - *Phys. Rev. Lett.*, 48:1252.

Hugrass, W.N., Jones, I.R., McKenna, K.F., Phillips, M.G.R., Storer, R.G., Tuczek, H. [1980] - *Phys. Rev. Lett.*, 44:1676.

Johnson, J.L., Dalhed, H.E., Greene, J.M., Grimm, R.C., Hsieh, Y.Y., Jardin, S.C., Manickam, J., Okabayashi, M., Storer, R.G., Todd, A.M.M., Voss, D.E., Weimer, K.E. [1979] - *J. Comput. Phys.*, 32:212.

Manickam, J., McCann B. [1977] - The Princeton Equilibrium and Stability Code. A Manual. Princeton University, Plasma Physics Laboratory.

Storer, R.G. [1982] - *Plasma Phys.*, 24:543.

Storer, R.G. [1983] - *Nucl. Instrum. Methods*, 207:135.

TABLE 1
PARAMETERS USED IN MODELLING THE ANSTO ROTAMAK

Case	δ	α	γ_1	β_1	γ_2	β_2
1	-0.5	4	-	-	-	-
2	0.9	10	0.5	2.0	0.25	10
3	0.48	4	0.4	2.8	0.41	3.2
4	3.0	5	0	-	0.06	5
5	2.6	3	0	-	0.05	3

TABLE 2
COMPARISON OF EXPERIMENTAL AND CALCULATED EQUILIBRIA

Case	X_a (cm)	X_s (cm)	p_a (Pa)	q_a	β_{pol}	W_p (J)	τ_E (μs)
1 Exp't	8.5	11.8	16	0			
Calc	9.3	13.1	15	0	2.7	0.16	5.1
2 Exp't	7.2	11.0	19	2.1			
Calc	9.0	12.8	17	0.7	1.7	0.14	4.6
3 Exp't	7.5	10.3	27	3.2			
Calc	9.2	12.7	24	2.2	2.2	0.23	5.5
4 Exp't	8.7	11.5	30	1.2			
Calc	9.6	12.4	26	1.5	2.5	0.19	4.9
5 Exp't	9.0	12.5	28	2.3			
Calc	10.1	12.8	25	1.7	2.7	0.16	4.2

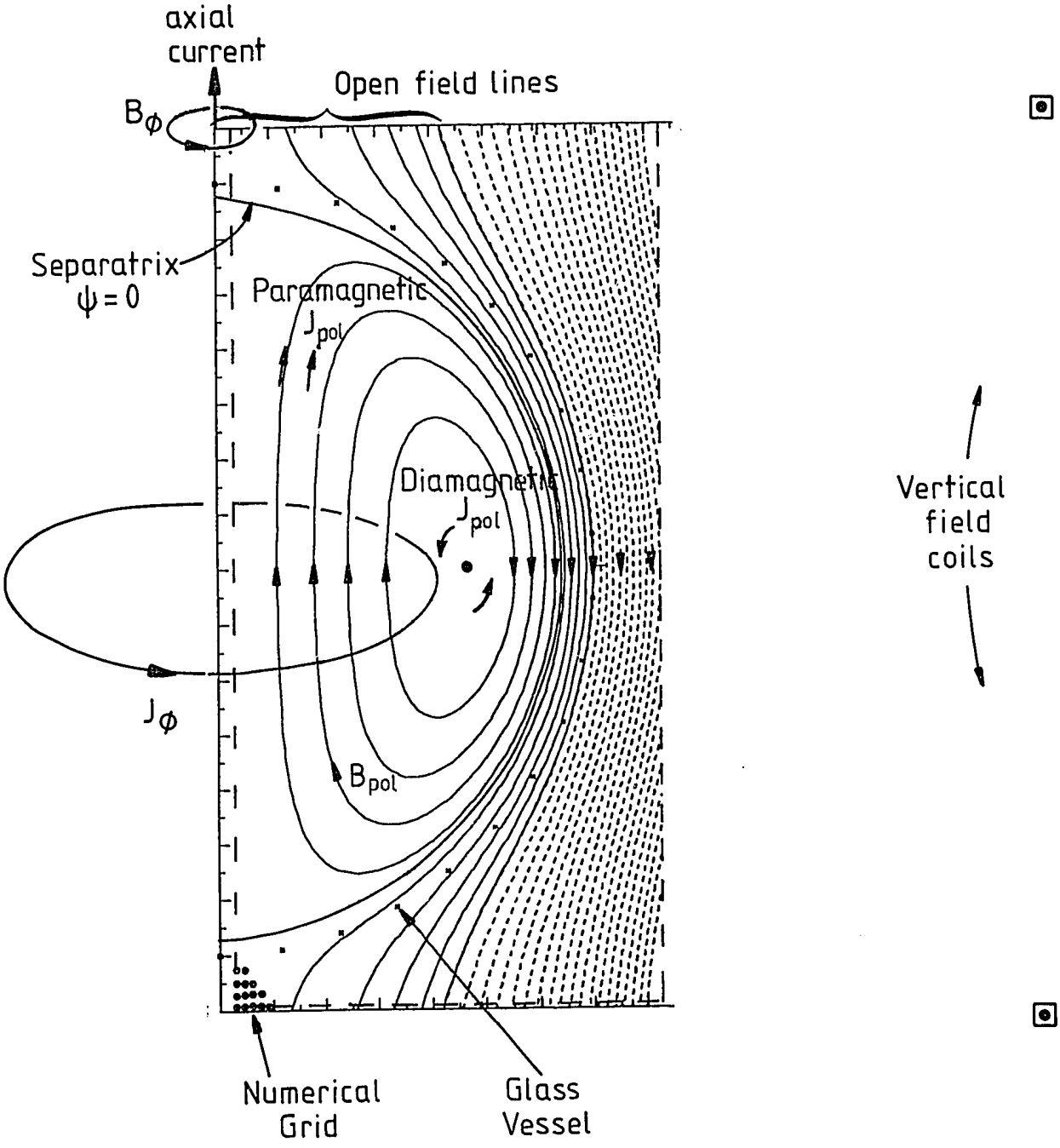

Figure 1 Schematic diagram of a rotamak equilibrium with B_ϕ (using the calculated poloidal flux contours for *Case 3*).

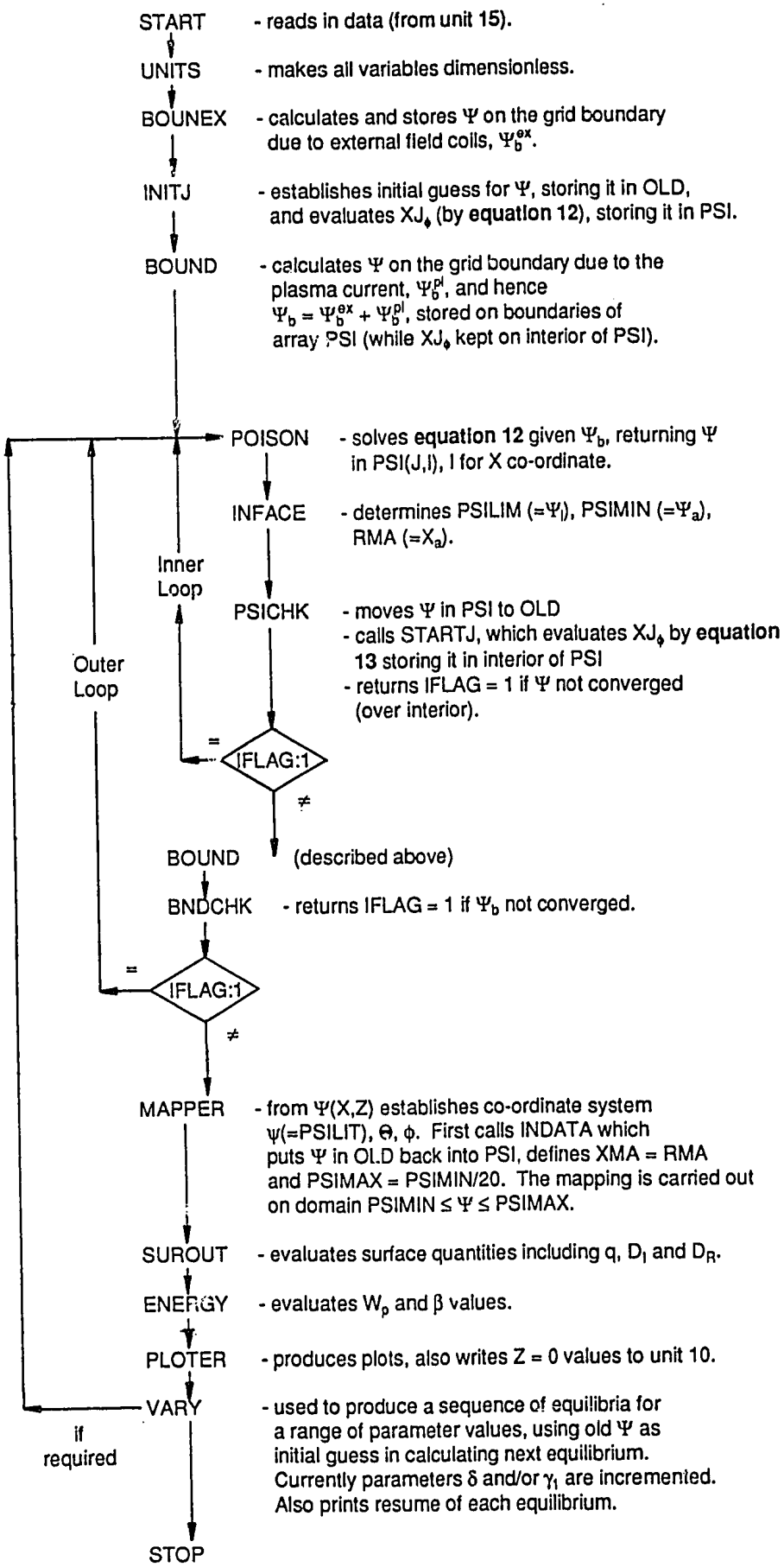

Figure 2 The equilibrium part of the PEST code

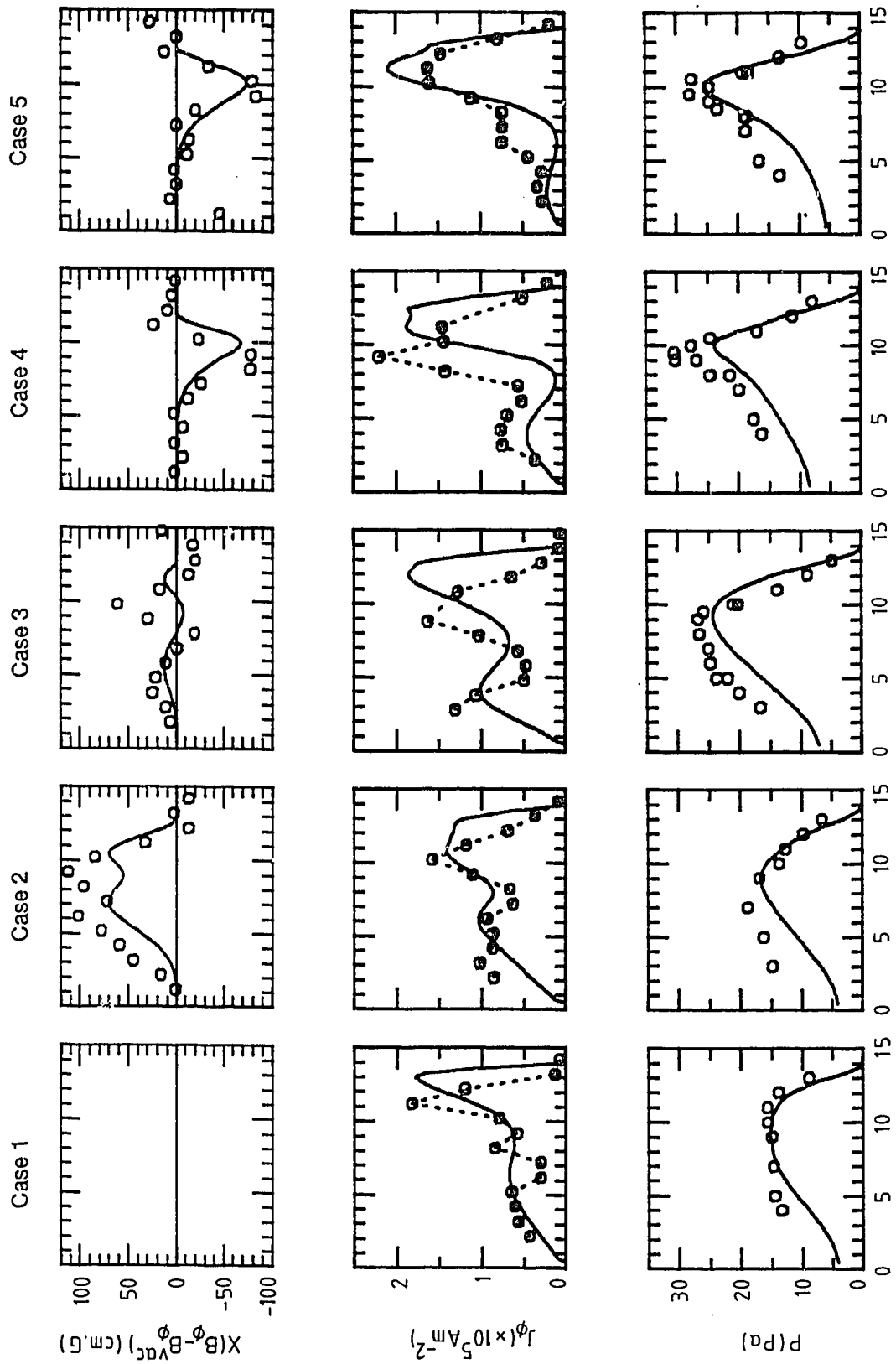

Figure 3 Comparison of profiles on Z = 0 of $X(B_\phi - B_\phi^{vac})$, J_ϕ and p: calculated (full line), experimental (dotted line)

APPENDIX A

AUXILIARY PROGRAMS

Two short computer programs have been written to help analyse the experimental data. Both take as input a file containing the experimental Ψ, J_ϕ and $g_{exp} = B_\phi/B_\phi^{vac}$ at a set of equispaced points on $Z = 0$.

Program PGPROG determines the $dp/d\Psi$ and g functions which should reproduce the experimental J_ϕ if the equilibrium is in pressure balance. First, linear interpolation is used on the experimental Ψ profile within the separatrix to obtain a set of pairs of X co-ordinates, (X_1, X_2) with $\Psi(X_1) = \Psi(X_2)$. For each pair of such points, $J_\phi(X_1)$ and $J_\phi(X_2)$ are found by linear interpolation, then **equation 3** provides a pair of simultaneous linear equations for $dp/d\Psi$ and $dg^2/d\Psi$. Thus $dp/d\Psi$ and g (after integrating from $g = 1$ at $\Psi = 0$) are obtained as functions of Ψ, over $\Psi < 0$. For $\Psi > 0$, *i.e.* outside the separatrix, it is merely assumed that $g = 1$ and $dp/d\Psi$ is again evaluated by **equation 3**.

The code plots the deduced $dp/d\Psi$ and g and fits them over $\Psi < 0$ with functions of **form 14a** and **14b** to yield parameters suitable for input to the PEST code. For $dp/d\Psi$ on $\Psi > 0$, **form 14c** with EXPP=2 was found to be adequate. The code also plots g_{exp} as a function of Ψ. Its consistency with the calculated g gives an indication of how close the equilibrium is to satisfying pressure balance.

For *Cases 2* to *5* in this report, the application of this program was not very successful. Unfortunately none of the PEST calculations converged for the parameter sets dictated by the above. However, rounding off the parameters of g produced *Case 3*. The results also pointed out how steep a $dp/d\Psi$ was required near the magnetic axis. The deduced g was generally of the same shape as g_{exp} (though this was only roughly a function of Ψ) but about half its magnitude. The compromise of improving the fit to g_{exp} while reducing the emphasis on J_ϕ led to the parameters used in the model equilibria.

Program PJB integrates the experimental $\mathbf{J} \times \mathbf{B}$ on $Z = 0$ to obtain a p profile (assumed zero at the vessel wall at $Z = 0$) for comparison with the measured p. Because of the large uncertainty in J_{pol} near $X = 0$, the results there should be ignored.

For each equilibrium given in this report, the maximum of the integrated p was always close to the maximum measured p.